Environmental Science and Pollution Research (2019) 26:22979–22989
https://doi.org/10.1007/s11356-019-05524-0

RESEARCH ARTICLE

An environment-friendly composite as an adsorbent for removal Cu (II) ions

Livy Laysandra[1,2] · Immanuel Joseph Ondang[1] · Yi-Hsu Ju[3] · Jindrayani Nyoo Putro[2] · Shella Permatasari Santoso[1,2] · Felycia Edi Soetarejo[1,2] · Suryadi Ismadji[1,2]

Received: 27 February 2019 / Accepted: 17 May 2019 / Published online: 10 June 2019

Abstract

The low-cost composite film was prepared by incorporating chitosan, berry soap fruit extract (rarasaponin), and bentonite as the raw materials. The produced chitosan/rarasaponin/bentonite (CRB) composite exhibits outstanding adsorption capability toward copper metal ions (Cu(II)). A series of static adsorption experiments were carried out to determine the isotherm and kinetic properties of CRB composite in the adsorption process. The adsorption equilibrium shows a good fit with the Langmuir isotherm model; the CRB composite has maximum uptake of Cu (II) of 412.70 mg/g; the kinetic adsorption data exhibit a good fit with the pseudo-second-order model. The thermodynamic parameters, $\Delta H°$, $\Delta G°$, and $\Delta S°$, obtained from the isotherm data indicate that the uptake of copper ions by CRB composite is more favored at low temperatures. This study shows that physicochemical modified adsorbent, namely CRB composite, can remove Cu (II) better than pristine adsorbent of AAB and chitosan. The CRB composite also shows potential reusability.

Keywords Ca-bentonite · Rarasaponin · Chitosan · Heavy metals · Copper ions · Isotherms · Kinetics · Thermodynamics · Adsorption

Introduction

Copper metal ions (Cu(II)) are one of the heavy metals most often found as water pollutants. The main source of Cu(II) pollutants mainly comes from wastewater from industries such as paper, textile, metal alloy, electroplating, and fertilizer (Li and Bai 2005). The presence of Cu(II) in the aquatic environment is a serious problem that requires more attention; this is due to its toxicity to humans and aquatic biota. Although Cu(II) is known as an essential nutrient for normal growth and metabolism, however, the excess amount of this metal can provoke various health disorders (Santore et al. 2001). Exposure of Cu(II) into the human body can occur both through the respiratory and digestive tracts. Accumulation of Cu(II) in the liver can cause mild disorders such as nausea, vomiting, abdominal, and muscle pain, to severe disorders such as gastrointestinal irritation, kidney damage, and liver damage (Liu et al. 2002).

At present, there are several methods available to control Cu (II) contamination in water and wastewater including chemical precipitation, electrochemical treatment, membrane filtration, electrodialysis, and adsorption. Hua et al. (2017) show that chemical precipitation method by using mechanically activated $CaCO_3$ can reduce Cu(II) in the water with a removal efficiency of 99.76% (Hua et al. 2017). Electrochemical treatment can reduce Cu(II) concentration in the pickling solution to below 100 mg/L (Karakaya et al. 2018). A recent study by Kontoudakis et al. (2018) showed

Responsible editor: Tito Roberto Cadaval Jr

Electronic supplementary material The online version of this article (https://doi.org/10.1007/s11356-019-05524-0) contains supplementary material, which is available to authorized users.

✉ Felycia Edi Soetarejo
felyciae@yahoo.com

✉ Suryadi Ismadji
suryadiismadji@yahoo.com

[1] Department of Chemical Engineering, Widya Mandala Surabaya Catholic University, Kalijudan 37, Surabaya 60114, Indonesia

[2] Department of Chemical Engineering, National Taiwan University of Science and Technology, No. 43, Sec 4, Keelung Rd, Da'an District, Taipei City 106, Taiwan

[3] Graduate Institute of Applied Science and Technology, National Taiwan University of Science and Technology, No. 43, Sec 4, Keelung Rd, Da'an District, Taipei City 106, Taiwan

that membrane filtration using polyethersulfonate and nylon membranes was able to remove sulfide-bound Cu in wine up to 40–90% (Kontoudakis et al. 2018). A Cu(II) removal percentage of 94.94–97.33% can be achieved by electrodialysis method using a cell packed with a pair of ion-exchange membranes and platinum electrodes (Mohammadi et al. 2004). Among the available methods, adsorption is the most preferred because of several appeals including ease of operation, favorable economic aspects, absence of the use of non-environmentally friendly chemicals, and absence of side waste or contaminants.

The benefit level of the adsorption depends entirely on the performance of the adsorbent. Adsorbents that have advantages such as high adsorption capacity, easy to use, inexpensive, harmless, and possible to reuse are still extensively developed today. For this purpose, many research focus on finding sophisticated composite materials that show great adsorption capabilities. A recent study by Torres-Caban et al. (2019) shows that composite beads adsorbent made from calcium-alginate/spent-coffee-grounds can adsorb 20.921 mg Cu(II)/g adsorbent (Torres-Caban et al. 2019). The carbon nanotubes/polypyrrole composite proposed in the study by Nyairo et al. (2018) have a maximum adsorption capacity of 24.39 toward Cu(II) (Nyairo et al. 2018). Zhou et al. (2017) show that the nano-MnO_2-biochar composite has a maximum adsorption capacity of 142.02 mg/g towards Cu(II) (Zhou et al. 2017). In this paper, a low-cost composite film prepared by combining chitosan/rarasaponin/bentonite is introduced; a considerable adsorption capability of the composite against Cu(II) is also shown.

The new adsorption method specifically emphasizes the use of biomolecules as an adsorbent to treat wastewater; this is because these materials are more environmentally friendly, non-toxic, viable, biodegradable, and capable to interact chemically or physically with various substances (Kurita 1998; Sankararamakrishnan and Sanghi 2006). One of the abundantly available biomolecules is chitosan. Chitosan has extraordinary characteristics such as hydrophobicity, biocompatible, biodegradable, antibacterial, non-toxic, and high mechanical strength (Inoue et al. 1999; Cervera et al. 2004). The hydroxyl (–OH) and amino ($–NH_2$) groups of chitosan are the main keys to chitosan modification. Modification of those functional groups allows chitosan to be formed into various forms such as film, fiber, hydrogel, membrane, nanoparticle, and microsphere (Nunthanid et al. 2001; Merrifield et al. 2004; Ngah and Fatinathan 2008; Zhou et al. 2009).

The preparation of chitosan/rarasaponin/bentonite (CRB) composite film and its capability for the removal of Cu (II) in aqueous solutions are reported in this paper. The incorporation of three materials (rarasaponin, bentonite, and chitosan) as a composite is worthy of study because of their beneficial existence, such as they are abounded in nature, inexpensive, and possible to be applied to industrial scale. The unique feature of the prepared composite due to molecular interactions of the three materials are discussed. The reusability and stability of the prepared composite are also investigated.

Materials and method

Materials

The raw materials for the preparation of composite are obtained from local areas in Indonesia; chitosan (85% deacetylated) was obtained from Biotech Surindo, West Java; Ca-bentonite was obtained from Punung Village, Pacitan, East Java, Indonesia; and *Sapindus rarak De Candole* was obtained from Klaten, Central Java. Analytical grade chemicals 1,5-diphenylcarbazide, H_2SO_4, $CuSO_4{\cdot}5H_2O$, Na_3PO_4, CH_3COOH, NaOH, NaCl, HCl, and C_6H_6 were purchased from Sigma Aldrich and used without further purification.

Preparation of rarasaponin-impregnated bentonite (rarasaponin-bentonite)

A total of 200 g of bentonite is activated by immersing it into 600 mL of 3 N H_2SO_4 solution for 2 h at a temperature of 373 K. The acid-activated bentonite (AAB) is cooled to room temperature and then continued with sonication for 1 h. AAB is rinsed continuously using deionized water until the pH of the rinse water reaches 6. AAB is then subjected to microwave irradiation with a strength of 700 W for 10 min. Next, the AAB is dried using a 378 K oven for overnight.

Sapindus rarak DC fruits are washed to remove dirt. The fruits are then dried at 353 K and pulverized into a particle size of + 180/− 200 mesh. Rarasaponin is obtained from the fruits by extracting dried-fruit powder with methanol in a mass-to-volume ratio of 1:3.75. Extraction was heated at 323 K for 60 min with a constant stirring 200 rpm. Subsequently, the supernatant was separated from the solid by centrifugation at 4900 rpm for 4 min. The methanol was removed from the supernatant by using rotary vacuum evaporator. The obtained rarasaponin crystal was collected from the evaporator flask and kept in an airtight container.

Rarasaponin-bentonite was prepared using a simple impregnation method. Briefly, 1 g of rarasaponin was dissolved in 100 mL deionized water. The solution was heated to 353 K for 30 min with a constant stirring 300 rpm. Subsequently, 10 g of AAB was added to the rarasaponin solution, and the mixture is stirred for another 30 min. The mixture was then irradiated in a microwave at a heating power of 700 W for 1 min. The rarasaponin-bentonite was dried at 378 K for 36 h, and then, the particle size was reduced to 100/200 mesh.

Preparation chitosan/rarasaponin/bentonite composite film

The chitosan/rarasaponin/bentonite (CRB) composite film was prepared according to the following procedure: 1 g of chitosan was dissolved in a 100 mL of 1 M acetic acid solution at 353 K for 1 h. Subsequently, 3 g of rarasaponin–bentonite was added to the chitosan solution. The mixture was heated at 353 K for 3 h with a constant stirring 500 rpm. The obtained CRB solution was then poured into the molding-tray with a liquid height of 1 mm and then dried at 333 K for 48 h. Dry CRB was placed in an airtight container until subsequent use.

Characterization of the adsorbents

The functional group of the adsorbent was characterized by using Fourier transform infrared (FTIR) spectroscopy (Shimadzu FTIR 8400S) at a wavenumber range of 4000–500 cm^{-1}. The X-ray diffraction (XRD) analysis was performed by using a Philips X'pert Xray diffractometer with a Cu $K_{\alpha 1}$ radiation at $\lambda = 0.1541$ nm. Nitrogen sorption isotherms were conducted by using a Micromeritics ASAP 2010 at a temperature of − 176 °C and a relative pressure range of 0.005 to 0.995. The point of zero charges (pHpzc) was determined by using the pH-drift method; the detailed procedure can be found elsewhere (Laysandra et al. 2019).

Adsorption experiments

The effect of temperature and pH in the removal of Cu(II) was studied. The temperature range studied is 303 to 343 K, while the pH range studied is 2 to 7, at a constant temperature of 303 K. The pH of the solution was adjusted by using 0.1 N sodium hydroxide or hydrochloric acid solution. An initial Cu(II) concentration of 500 mg/L and adsorbent mass of 0.3 g was used, and the adsorption was conducted for 4 h in a thermostated shaker water bath. Removal efficiency is expressed as a percentage value calculated using the following equation:

$$\%\text{Removal} = \frac{C_o - C_e}{C_o} \times 100\% \quad (1)$$

The adsorption isotherms of Cu (II) on AAB, chitosan, and CRB composite were obtained isothermally at 303, 323, and 343 K. A known amount of adsorbents (0.1–1.0 g) was added into iodine flasks (each contains 100 mL of Cu (II) solution with the concentration of 500 mg/L). The flasks were placed into the shaker water bath and shaken at 200 rpm for 4 h. The solid was separated from the solution by centrifugation at 5000 rpm for 10 min. The amount of Cu(II) adsorbed at equilibrium condition (q_e) was determined according to the eq. (2).

$$q_e = \frac{(C_o - C_e)}{m} \times V \quad (2)$$

where C_o is the initial concentration of heavy metal in the solution, mg/L; C_e is the equilibrium concentration of heavy metal, mg/L; V is the volume of the solution, L; and m is the mass of the adsorbent, g. As for the adsorption kinetics, three different Cu(II) initial concentrations (100, 300, and 500 mg/L) and 0.3 g adsorbent was used. The sampling was done at a certain time interval. The concentration of Cu(II) ions was determined by using the 1,5-diphenylcarbazide method. The concentration was determined by measuring the absorbance at 540 nm using a UV-Vis spectrophotometer (UV-1700 PharmaSpec, Shimadzu). The detailed procedure can be found elsewhere (Turkington and Tracy 1958).

Reusability test

Reusability of the prepared composite was tested by conducting six adsorption-desorption cycles at a temperature of 303 K. Adsorption was conducted by using 0.3 g adsorbent and initial Cu(II) concentration of 500 mg/L for 4 h. Desorption was carried out in 0.5 mol/L HCl solution as the eluent; the Cu(II) loaded-adsorbent is gently shaken in eluent for 4 h, then the intact adsorbent was taken and used for another consecutive cycle.

Result and discussion

Characterization of the adsorbents

Surface functional groups of the adsorbents analyzed using FTIR are presented in Table S1. The characteristic peaks of each composite raw materials were observed to confirm their involvement in the composite structure (Table 1). The main characteristic peaks of rarasaponin which have been identified for the C=O stretch of the carbonyl ester group, C–H bend at hydroxyl group, C–O stretch of deacylated carbonyl group, and C=C stretch of aromatic rings, are observed at wavenumbers 1699.17, 1361.65, 1286.43, and 1056.92 cm^{-1}, respectively. The main peaks of chitosan which correspond to C=O in amide group, $–NH_2$ in the amino group, –NH bend, O–H vibration, and C–H vibration are observed at 1768.60, 1596.95, 1506.3, 1423.37, and 1325.01 cm^{-1}, respectively. The main peaks of AAB associated with the silanol and alumina group were observed at wavenumbers 1051.13, 935.41, 671.18, 478.31, and 453.24 cm^{-1}; where they refer to Si–O–Si stretch in tetrahedral layer, Al–Al–OH bend, Si–O stretch on silica and quartz, Si–O–Al bend in octahedral Al, and Si–O–Si bend, respectively. Enhanced characteristic peaks derived from the raw materials (rarasaponin, chitosan, and AAB) were observed in CRB

Table 1 The FTIR analysis of raw matrials, rarasaponin, chitosan, and CRB composite

Functional Group	Rarasaponin	Chitosan	AAB	CRB composite
O–H stretch (alcohols or phenols)	-	-	3847.72	3865.08
O–H stretch of silanol (Si–OH) groups	-	-	2929.67	2935.46
C=O in amide group	-	1768.6	-	1656.74
C=O stretch (Ester carbonyl group)	1699.17	-	-	1629.74
O–H bend, for adsorbed H_2O at bentonite interlayer	-	-	1647.10	-
NH_2 in amino group	-	1596.95	-	1539.09
NH bending vibration in amide group	-	1506.30	-	1413.72
O–H vibration in amide ring	-	1423.37	-	-
C–H bend bonded with hydroxyl group	1361.65	-	-	1382.87
C–H vibration in amide ring	-	1325.01	-	-
C–O stretch of deacylated carbonyl group	1286.43	-	-	1286.43
C=C stretch (aromatic rings group)	1056.92	-	-	-
Si–O–Si stretch of the tetrahedral layer	-	-	1051.13	1029.92
Al–Al–OH bend	-	-	935.41	-
Si–O stretching of silica and quartz	-	-	671.18	659.61
Si–O–Al bend (for octahedral Al)	-	-	478.31	503.39
Si–O–Si bend	-	-	453.24	472.53

composite, suggesting that raw materials were successfully embedded in the CRB composite. Some of the enhanced characteristic peaks are as follows: the presence of carbonyl groups from rarasaponin is indicated by the wavenumbers 1699.17 and 1286.43 cm^{-1}; amide groups from chitosan are indicated by the wavenumbers 1656.74 and 1413.72 cm^{-1}; and silanol groups from AAB indicated by the wavenumbers 2935.46, 1029.92, 659.61, 503.39, and 472.53 cm^{-1}.

The crystallinity of AAB and CRB composite is characterized by XRD analysis; the diffractograms are presented in supplementary data Fig. S1. The diffraction peaks contributed to the crystal planes of montmorillonite is observed for both AAB and CRB; specifically, at $2\theta = 6.1$, 22.1, 30.1, and 35.9° for AAB, at $2\theta = 5.8$, 19.8, 31.3, and 36.2 for CRB composite. The reduced intensity of 001 planes for CRB compared to AAB suggests the intercalation of rarasaponin; moreover, the typical 001 diffraction plane shows an alteration from 6.1° (in AAB) to 5.8° (in CRB). The basal spacing measurement for AAB at $2\theta = 6.1°$ is 1.45 nm, and for CRB at $2\theta = 5.8°$ is 1.52 nm. The increase in basal is due to the intercalation of rarasaponin in the interlayer of montmorillonite. The characteristic peaks in other 2θ belong to a crystal plane of quartz, kaolinite, and illite.

Nitrogen sorption isotherms of AAB and CRB are provided in supplementary data Fig. S2. A combination of sorption isotherm plot type I and IV was observed for AAB, Fig. S2(a). The type I isotherm behavior indicated by a steep pore filling with volume adsorbed of 25 cm^3/g at a low relative pressure (P/P_0), this characteristic indicates the presence of microporous structure. Transition to the type IV isotherm at higher P/P_0 with larger pore filling indicate the presence mesoporous structure in AAB. The presence of micro-mesoporous in AAB is supported by the DFT pore size distribution (5–150 A or 0.5–15 nm), as shown in the inset in Fig. S2(a). The nitrogen sorption isotherm for CRB also show a combination of isotherm plot type I and IV but with the steeper pore filling at high P/P_0. The steeper pore filling suggests a more complex structure of the adsorbent, which is most likely due to the incorporation of rarasaponin and chitosan into AAB creating a multilayered structure. Furthermore, a nearly vertical plot at P/P_0 close to 0.99 indicates delayed desorption due to the multilayer structure of CRB (Lu et al. 2017; Sotomayor et al. 2018).

The formation mechanism of the CRB composite

CRB composite was prepared by combining the rarasaponin-impregnated bentonite with chitosan in an acidic solution. The formation mechanism of the CRB composite is graphically presented in Fig. 1; the two main mechanisms are the impregnation of bentonite by rarasaponin and particle incorporation by chitosan. The impregnation of bentonite-rarasaponin occurs due to a charge difference between the two particles. Bentonite used in impregnation has been acid-activated; the activation process causes the silanol group, Si–OH, to be protonated to $Si–OH_2^+$. As for rarasaponin, the dissolution of compound initiates disengagement of two acyl groups ($–C_2H_3O^+$) and leaving two negatively charged oxygen atoms. Negatively charged rarasaponin attacks positively charged bentonite so that the impregnation process occurs (Kurniawan et al. 2011). The acidic chitosan solution was added before the formation of the CRB composite. The acidic environment causes the protonation of the amine groups in chitosan; this protonated amine then forms a bond with the deacylated rarasaponin. Molecular interaction also occurs between chitosan and bentonite, where the van der Waals hydrogen bond is the most likely interactions. The interaction between the three molecules (chitosan, rarasaponin, bentonite) leads to the formation of chitosan/rarasaponin/bentonite (CRB) composite.

Adsorption studies

Influence of temperature

The adsorption capability of AAB, chitosan, and CRB composite at various temperature is given in Fig. 2. It is obvious

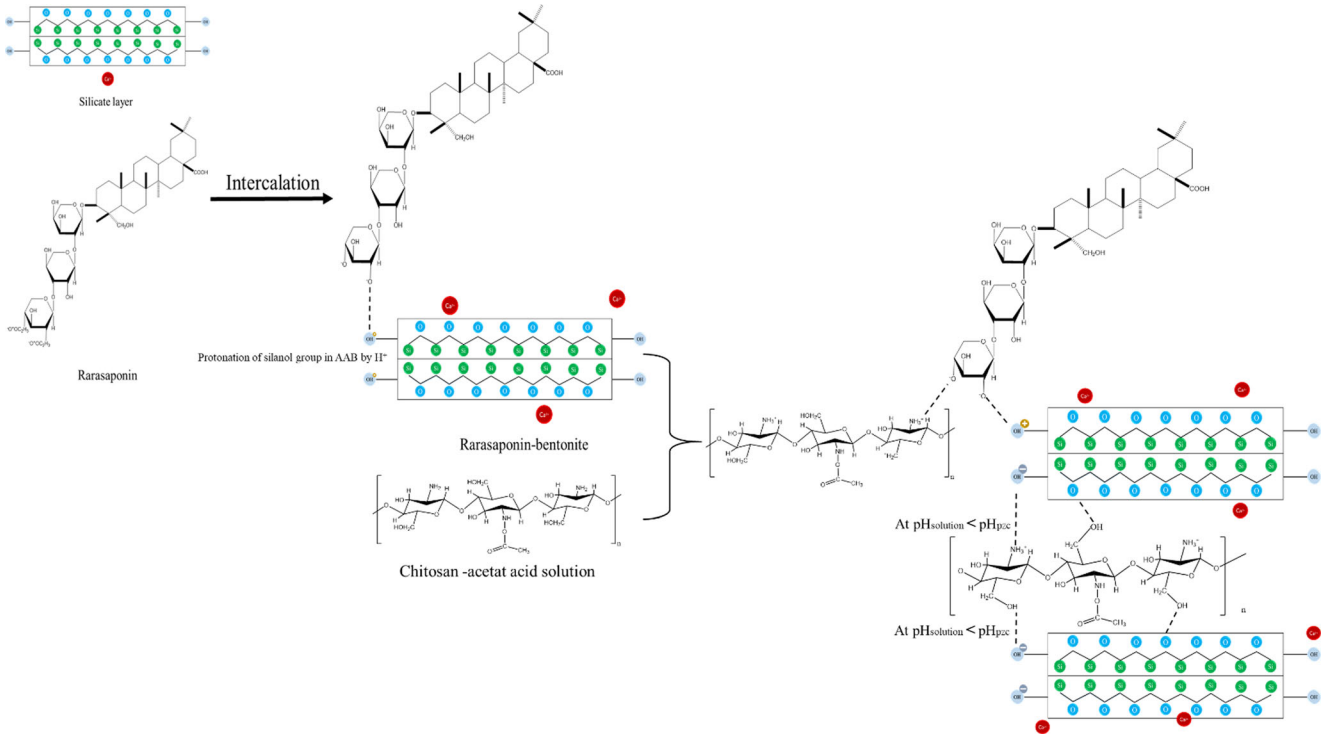

Fig. 1 The formation mechanism of CRB composite film (octahedral sheets are not shown in silicate structures)

that the CRB composite exhibits better adsorption capability compared to the parent materials. CRB has the highest removal efficiency of 88.59% at 303 K; removal efficiency decreases as temperature increases. The opposite phenomenon is observed for AAB and chitosan; increase in temperature causes a decrease in removal efficiency. The highest removal efficiency for AAB and chitosan is 28.83 and 68.70%, respectively, at 343 K.

The temperature has two main effects in the adsorption process: (1) an increase in temperature enhances the rate of diffusion of copper ions to the adsorbent; (2) if chemisorption is the control mechanism, the increase in temperature will enhance the uptake of Cu(II). In this study, the increase of temperature has a negative impact on the removal of Cu (II) by CRB. This is due to the attractive force between Cu(II) ions, and the surface of the adsorbent weakens at high temperatures so that Cu(II) ions can escape easily. Furthermore, the kinetic energy of Cu(II) ions increases at higher temperature thereby increasing the tendency of ions to escape from the adsorbent (Aksu and Kutsal 1991; Horsfall and Spiff 2005). The removal efficiency of Cu(II) by CRB decreases as the temperature is raised indicating that the removal process is exothermic.

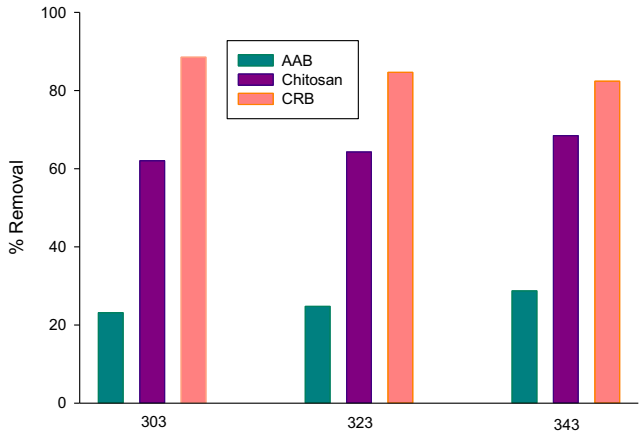

Fig. 2 Adsorption capability of raw materials and CRB composite at various temperatures

Influence of initial pH

Acidity or alkalinity of the solution controls the interaction between adsorbent and adsorbate in an adsorption process. As shown in Fig. 3, the adsorption of Cu(II) in the pH range 2 to 7 was studied to examine the effect of alkalinity in the adsorption process. It is noted that at acidic pH below 5, adsorption of Cu(II) by AAB and CRB is poor. The highest adsorption of Cu(II) occurs at pH 6 for AAB and pH 5 for CRB, where the maximum adsorption is 23.05 and 62.50 mg/g for AAB and CRB, respectively. Adsorption of Cu(II) by AAB and CRB decreases as the pH is increased further. The adsorption characteristic under different alkalinity conditions can be explained by examining the electrical potential difference between the adsorbate and adsorbent molecules.

The electrical potential of the adsorbent can be properly described from point zero charges (pHpzc) (Komulski and Saneluta 2004). The net positive charge on the surface of

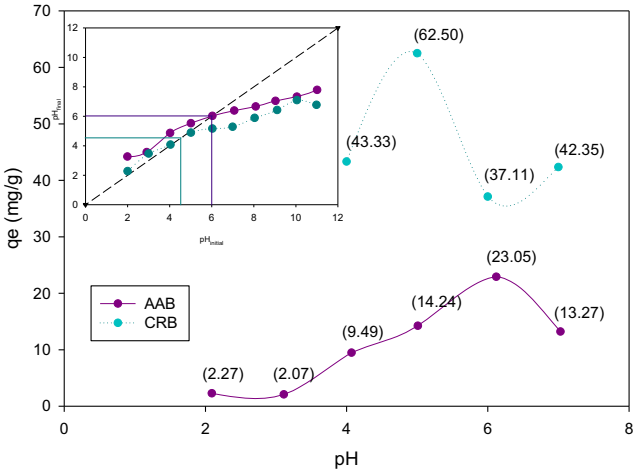

Fig. 3 The influence of pH on the adsorption of Cu(II) onto AAB and CRB

adsorbent is achieved as the pH < pHpzc, isoelectric point is achieved as pH = pHpzc, and net negative charged is achieved as the pH > pHpzc. As shown in the inset of Fig. 5, pHpzc of AAB is 6.01 and for CRB is 4.54. This means that at pH below 5, the surface charge of AAB and CRB is positive due to the attack of H^+ contained in the acidic solution; H^+ ions and Cu(II) ions then compete for the active site of the adsorbent which caused drawback of adsorption of Cu(II). At the best Cu(II) adsorption pH, when pH of the solution exceeds pHpzc, the number of active sites available for binding of heavy metal ions increases because H^+ in the solution decreases which leads to an increase in adsorption of Cu(II) (Yu et al. 2016). Moreover, at pH above pHpzc, the surface charge of the adsorbent is negative while Cu(II) ion tends to be presented in the form of its divalent ion accompanied by several hydroxides species such as $CuOH^+$, $CuCO_3$, $CuHCO_3^+$, and $Cu(OH)_2$. Electrostatic difference between adsorbent and Cu(II) promotes the adsorption of Cu(II). A decrease in adsorption at a greater pH (> 5 for CRB and > 6 for AAB) is caused by the presence of excess hydroxide ions which cause both the adsorbent and adsorbate molecules to be negatively charged. Cu(II) ions tend to exist as $Cu(OH)_3^-$ and $Cu(OH)_4^{2-}$ in solutions with an excessive amount of hydroxide ions (Khan and Wahab 2007). The repulsive force becomes dominant because both molecules possess the same electrostatic charge (Lu et al. 2017).

Adsorption isotherm

The adsorption isotherms of Cu(II) on AAB and CRB are depicted in Fig. 4. The experimental adsorption equilibria were correlated using two well-known isotherm equations namely Langmuir and Freundlich. The Langmuir equation is developed according to the following simple assumptions: monolayer adsorption, identic adsorption sites, localized adsorption, and constant adsorption energy (Langmuir 1918). The mathematic expression of the Langmuir can be written as

$$q_e = q_m\left(\frac{K_L C_e}{1 + K_L C_e}\right) \tag{3}$$

The parameter q_m in Eq. (3) represents the maximum amount of adsorbate adsorbed by the adsorbent (mg/g). The affinity of the adsorbate towards the surface of adsorbent is represented by the K_L parameter (L/mg).

The Freundlich equation represents the adsorption of gases or liquids on the heterogeneous surface of adsorbents. This equation can be used to analyze the heterogeneity of the adsorbent surface and the energy of its active sites (Freundlich 1906). Freundlich equation has the following mathematical form:

$$q_e = K_F C_e^{\,1/n_F} \tag{4}$$

where K_F ((mg/g).(L/mg)$^{-n}$) and n_F are the Freundlich adsorption capacity and heterogeneity constant for the adsorption system, respectively.

The fitting of experimental and calculated data was conducted using the non-linear least square method; the results are graphically presented in Fig. 4 while the calculated parameters are given in Table 2. Based on the values of R^2, the data fitting using Langmuir equation is better than Freundlich, indicating that the adsorption of Cu(II) on CRB and AAB occurs at the homogeneous sites of the adsorbent (Lu et al. 2017). The isotherm adsorption was done at three different temperatures of 303, 323, and 343. The maximum adsorption capacity of Cu (II) by CRB composite at 303, 323, and 343 K are 412.70, 386.47, and 359.60 mg/g, respectively. It is also proven from the isotherm data fitting that adsorption by CRB occurs exothermically. The data fitting using the Freundlich equation supported exothermic adsorption process by CRB, in which the K_F value decreased with the increase of temperature. Comparison of CRB adsorption capacity against other adsorbents on Cu(II) is shown in Table S2. CRB exhibits an outstanding adsorption capacity compared to the other similar adsorbents indicates that CRB can be a potential adsorbent for Cu(II).

Adsorption kinetics

The pseudo-first (Corbett 1972) and pseudo-second-order (Ho and McKay 1999) equations were employed to correlate the kinetic experimental data. The pseudo-first and pseudo-second-order equations are expressed as eq. (5) and (6), respectively:

$$q_t = q_{e1}(1 - exp(-k_1 t)) \tag{5}$$

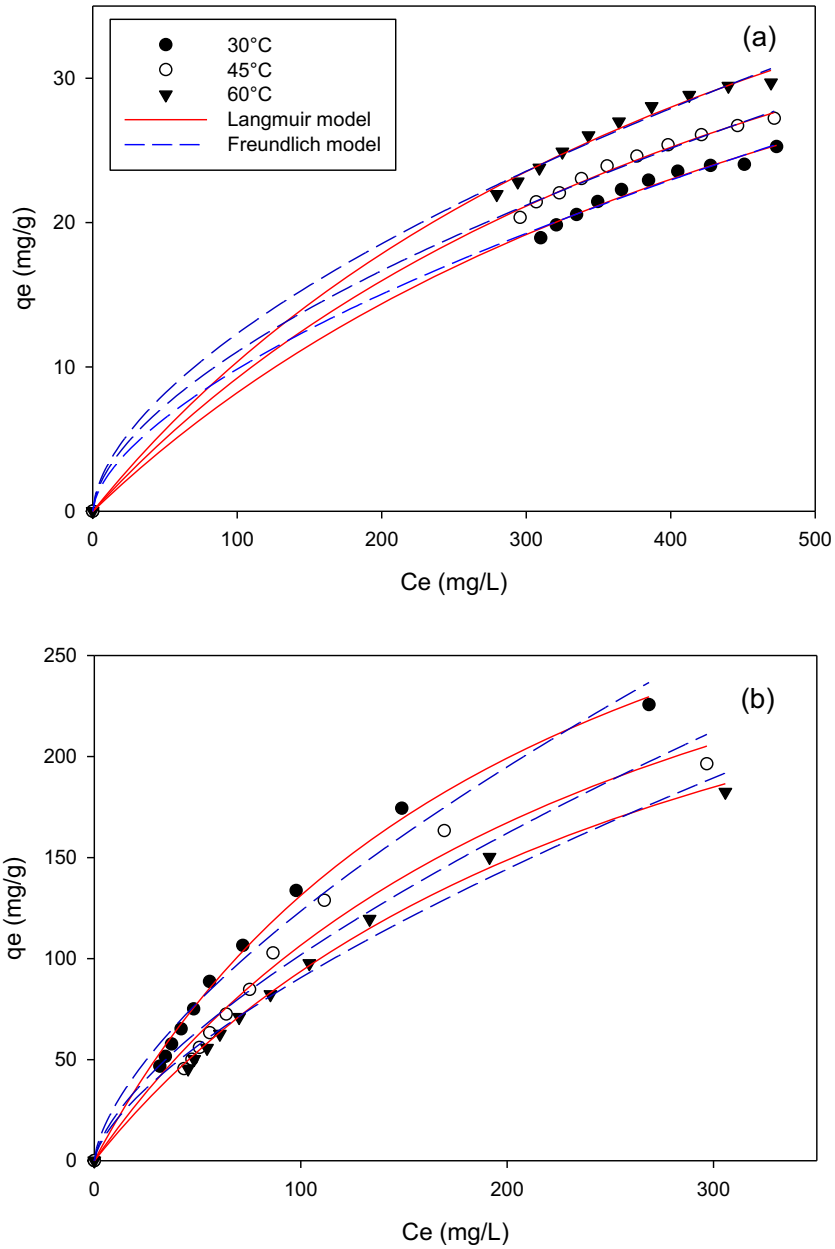

Fig. 4 Adsorption isotherms of Cu(II) on **a** AAB and **b** CRB

Table 2 The parameters of Langmuir and Freundlich equations for the adsorption of Cu(II) on AAB and CRB

Adsorbent and temperature	Langmuir			Freundlich		
	q_m (mg/g)	K_L (L/mg)	R^2	K_F (mg/g)(mg/L)$^{-n}$)	n_F	R^2
AAB						
303 K	57.40	0.0017	0.9968	0.5967	1.6415	0.9962
323 K	59.57	0.0018	0.9984	0.7233	1.6822	0.9978
343 K	64.70	0.0019	0.9969	0.8151	1.6954	0.9958
CRB						
303 K	412.70	0.0047	0.9958	5.9704	1.5202	0.9799
323 K	386.47	0.0038	0.9785	4.6719	1.4942	0.9551
343 K	359.60	0.0035	0.9964	4.1063	1.4887	0.9841

$$q_t = q_{e2}\left(\frac{q_{e2}k_2 t}{1 + q_{e2}k_2}\right) \quad (6)$$

where q_t (mg/g) shows the uptake of heavy metal adsorbed by the adsorbent at a certain time, t (min). Parameters k_1 (1/min) and k_2 (g/mg.min) are the time constant for the pseudo-first and pseudo-second-order models, respectively. Parameters q_{e1} and q_{e2} are the amounts of Cu (II) adsorbed at equilibrium condition. The effect of initial Cu(II) concentration on the adsorption was also investigated in the kinetic study, where the initial Cu(II) concentration studies are 150, 300, and 500 ppm.

The fitting on the adsorption kinetics data using the pseudo-first and pseudo-second-order equations are given in Fig. 5; the parameters of both equations are presented in Table 3. The R^2 value for pseudo-second-order fitting is closer to 1 compared to that pseudo-first-order fitting, indicates that the pseudo-second-order equation represents the kinetic data better. Better fitting to the pseudo-second-order equation shows that the interaction between the adsorbate and the adsorbent is chemisorption controlled. The fact that the adsorption capacity decreases as the temperature increases indicates that the chemisorption is exothermic in this study (Arshadi et al. 2014). The effect of initial Cu(II) ion concentrations to the adsorption is also illustrated in Fig. 5. The increase in Cu(II) adsorption capacity with increasing Cu(II) initial concentrations indicates that the concentration gradient plays an important

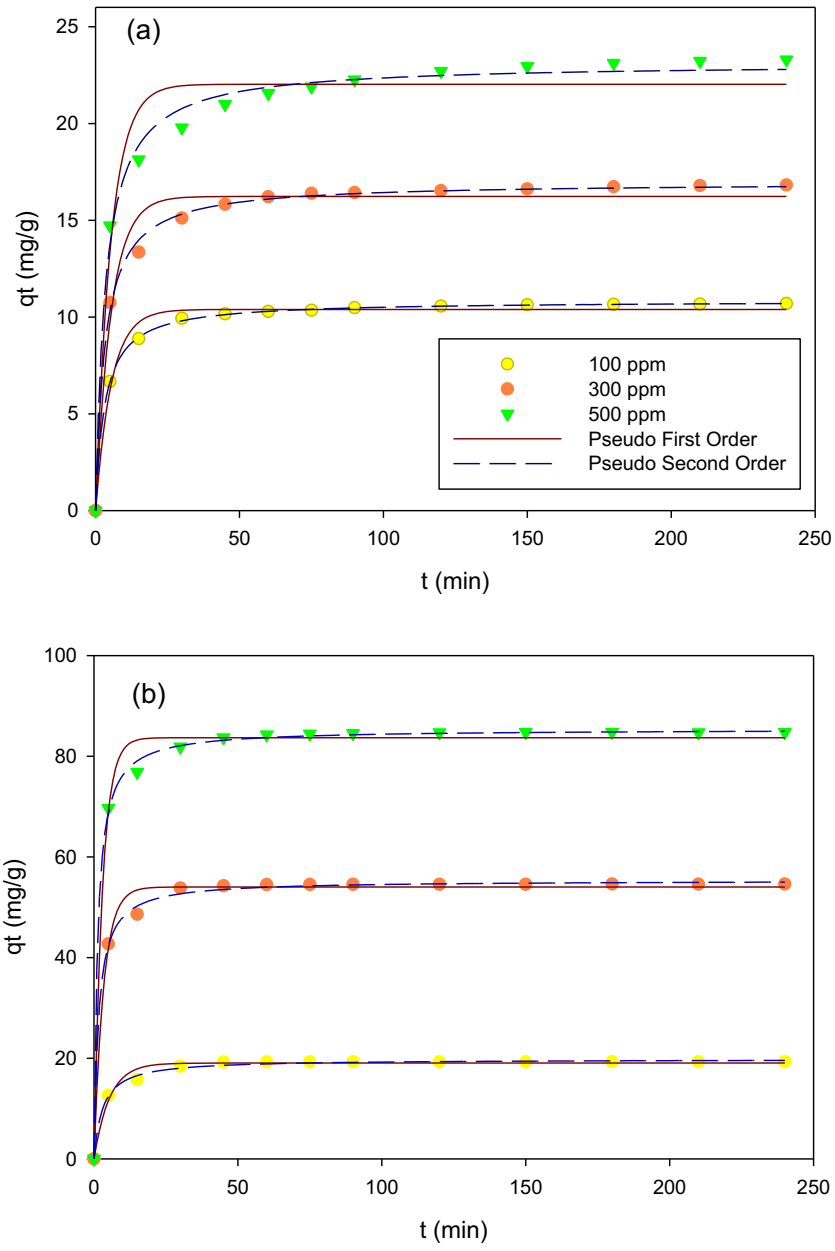

Fig. 5 Adsorption kinetics of Cu(II) on **a** AAB and **b** CRB

Table 3 The parameters of the pseudo-first and pseudo-second-order models for the adsorption of Cu (II) on AAB and CRB (T = 30 °C and mass adsorbent = 0.5 g)

The initial concentration of Cu (II) (ppm)	Experimental result	Pseudo-first order			Pseudo-second order		
	qe_{exp} (mg/g)	k_1 (min^{-1})	q_{e1} (mg/g)	R^2	k_2 (mg g^{-1} min^{-1})	q_{e2} (mg/g)	R^2
AAB							
100	10.6993	0.1832	10.3986	0.9863	0.0293	10.8463	0.9998
300	16.8234	0.1853	16.2349	0.9738	0.0184	16.9666	0.9975
500	23.2965	0.1880	22.0302	0.9592	0.0128	23.1194	0.9926
CRB							
100	19.2690	0.1866	19.0343	0.9816	0.0171	19.8003	0.9953
300	54.5788	0.3003	54.0150	0.9905	0.0118	55.3369	0.9980
500	84.7710	0.3493	83.6714	0.9921	0.0098	85.3768	0.9990

role in the adsorption process. Cu(II) ions in solution provide a driving force that supports mass transfer between adsorbate and adsorbent molecules; the higher the initial concentration of Cu(II) causes the resistance to mass transfer to weaken. Moreover, the weakening of resistance to mass transfer encourages electrostatic interactions between metal ions and adsorbent so that the adsorption capacity increases (Kurniawan et al. 2011; Arshadi et al. 2014).

Thermodynamic parameters

Thermodynamic parameters, specifically enthalpy change ($\Delta H°$), entropy change ($\Delta S°$), and Gibbs free energy change ($\Delta G°$), are crucial parameters in determining the spontaneity and suitability of an adsorption process. The value of $\Delta G°$ can be calculated using the following equation:

$$\Delta G° = -RT\ln K \tag{7}$$

In a constant pressure and temperature, the relation of $\Delta G°$, $\Delta H°$, and $\Delta S°$ can be expressed as the following equation:

$$\Delta G° = \Delta H° - T.\Delta S° \tag{8}$$

The values of $\Delta H°$ and $\Delta S°$ are shown by the slope and intercept of the Van't Hoff plot ln K vs $1/T$:

$$\ln K = \frac{\Delta S°}{R} - \frac{\Delta H°}{RT} \tag{9}$$

where K is the equilibrium constant that can be obtained by plotting ln (q_e/C_e) vs. C_e then extrapolating to zero. The other parameters, R is gas constant (8.314 J/ mol.K), and T is absolute temperature (K).

The calculated thermodynamic parameters are given in Table 4. The negative $\Delta G°$ confirms the feasibility and spontaneity of Cu(II) adsorption by CRB; however, $\Delta G°$ becomes more positive as temperature increases indicating that spontaneity declines at a higher temperature. Exothermic behavior of Cu(II) adsorption on CRB is shown from the negative $\Delta H°$ value, asserting that the adsorption of Cu(II) is more suitable at low temperatures. Positive $\Delta S°$ indicates randomness in the immobilization of metal ions on the active sites of the adsorbent in the adsorption process which allows for spontaneous adsorption. In the adsorption of Cu(II) by AAB, the process also runs spontaneously as indicated by negative $\Delta G°$. The positive value of $\Delta H°$ indicates endothermic adsorption of Cu(II) onto AAB. The affinity of Cu(II) towards AAB is weaker than towards CRB as indicated by the higher positive $\Delta S°$ of CRB.

Reusability and stability of CRB adsorbent

The reusability of CRB adsorbent was investigated by performing adsorption-desorption cycles at 303 K. As

Table 4 The thermodynamic parameters for the adsorption of copper (II) ions on AAB and CRB

Temperature (K)	AAB			CRB		
	$\Delta G°$ kJ/ mol	$\Delta H°$ kJ/ mol	$\Delta S°$ J/mol·K	$\Delta G°$ kJ/ mol	$\Delta H°$ kJ/ mol	$\Delta S°$ J/mol·K
303	− 6.15	3.5	5.13	− 1.37	− 2.45	87.2
323	− 6.58			− 0.63		
343	− 6.90			− 0.41		

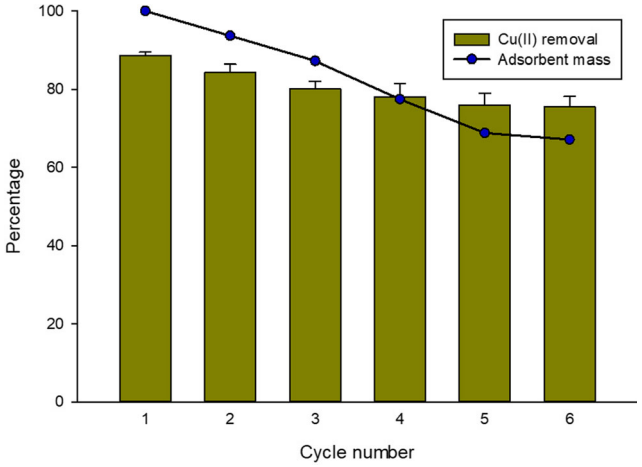

Fig. 6 Reusability and degradation test of CRB composite

shown in Fig. 6, the CRB composite was still capable of removing 75.5% Cu(II) after 6 consecutive cycles. However, the decrease in CRB mass caused by particle detachment was also observed in each cycle. After six cycles, 82.5% of the adsorbent mass remains; some parts of the CRB adsorbent are detached from the starting material which is due to the chitosan degradation. It is evident that CRB composite can be reused and regenerated even though there is a decrease in the removal efficiency of Cu (II) at each regeneration stage accompanied by the breakdown of CRB particles. Apart from the breakdown of CRB composite, it has several advantages, that is high adsorption ability compared to some reported adsorbents (Table S2), inexpensive raw materials, and environmentally friendly properties.

Conclusion

A new composite material with high adsorption capacity towards Cu(II) was successfully prepared by combining chitosan–rarasaponin–bentonite (CRB) through a straightforward impregnation and irradiation process. The adsorption of Cu(II) onto CRB composite is an exothermic process, the maximum adsorption capacity of CRB is found to be 412.70 mg/g at 303 K. The isotherm and kinetics adsorptions are well represented by Langmuir and pseudo-second-order model. The negative values of $\Delta G°$ confirm the feasibility and the spontaneity of Cu (II) adsorption by CRB. In addition to its high adsorption capacity, CRB can be reused and regenerated. CRB still able to remove up to 82.5% of Cu(II) after 6 adsorption-desorption cycles.

Funding information Financial support from Indonesia Ministry of Research and Technology and Higher Education through PDUPT research scheme.

References

Aksu Z, Kutsal TA (1991) A bioseparation process for removing Pb(II) ions from wastewater by using *C. vulgaris*. J Chem Technol Biotechnol 52:108–118

Arshadi M, Amiri MJ, Mousavi S (2014) Kinetic, equilibrium and thermodynamic investigations of Ni(II), cd(II), cu(II) and co(II) adsorption on barley straw ash. Water Res Ind 6:1–17. https://doi.org/10.1016/j.wri.2014.06.001

Cervera MF, Heinämäki J, Räsänen M, Maunu SL, Karjalainen M, Acosta OMN, Colarte AI, Yliruusi J (2004) Solid-state characterization of chitosans derived from lobster chitin. Carbohydr Polym 58:401–408. https://doi.org/10.1016/j.carbpol.2004.08.017

Corbett JF (1972) Pseudo first-order kinetics. J Chem Educ 49:663. https://doi.org/10.1021/ed049p663

Freundlich HMF (1906) Over the adsorption in solution. J Phys Chem 57:385–471

Ho YS, McKay G (1999) Pseudo-second order model for sorption processes. Process Biochem 34:451–465. https://doi.org/10.1016/S0032-9592(98)00112-5

Horsfall M, Spiff AI (2005) Effects of temperature on the sorption of Pb^{2+} and Cd^{2+} from aqueous solution by *Caladium bicolor* (wild cocoyam) biomass. Electron J Biotechnol 8:162–169

Hua H, Li X, Huang P, Zhang Q, Yuan W (2017) Efficient removal of copper from wastewater by using mechanically activated calcium carbonate. J Environ Manag 203:1–7. https://doi.org/10.1016/j.jenvman.2017.07.066

Inoue K, Yoshizuka K, Ohto K (1999) Adsorptive separation of some metal ions by complexing agent types of chemically modified chitosan. Anal Chim Acta 388:209–218. https://doi.org/10.1016/S0003-2670(99)00090-2

Karakaya E, Aras MS, Erdoğan M, Karagül SÇ, Ersoy MK, Karakaya İ (2018) An electrochemical procedure for copper removal from regenerated pickling solutions of steel plants. Energy technology 2018. The Minerals, Metals & Materials Series. Springer, Cham. https://doi.org/10.1007/978-3-319-72362-4_24

Khan MN, Wahab MF (2007) Characterization of chemically modified corncobs and its application in the removal of metal ions from aqueous solution. J Hazard Mater 141:237–244. https://doi.org/10.1016/j.jhazmat.2006.06.119

Komulski M, Saneluta C (2004) Point of zero charge/isoelectric point of exotic oxides: Tl_2O_3. J Colloid Interface Sci 280:544–545. https://doi.org/10.1016/j.jcis.2004.08.079

Kontoudakis N, Mierczynska-Vasilev A, Guo A, Smith PA, Scollary GR, Wilkes EN, Clark AC (2018) Removal of sulfide-bound copper from white wine by membrane filtration. Aust J Grape Wine R 25:53–61. https://doi.org/10.1111/ajgw.12360

Kurita K (1998) Chemistry and application of chitin and chitosan. Polym Degrad Stab 59:117–120. https://doi.org/10.1016/S0141-3910(97)00160-2

Kurniawan A, Sutiono H, Ju YH, Soetaredjo FE, Ayucitra A, Yudha A, Ismadji S (2011) Utilization of rarasaponin natural surfactant for organo-bentonite preparation: application for methylene blue removal from aqueous effluent. Microporous Mesoporous Mater 142:184–193. https://doi.org/10.1016/j.micromeso.2010.11.032

Langmuir I (1918) The adsorption of gases on plane surfaces of glass, mica and platinum. J Am Chem Soc 40:1361–1403. https://doi.org/10.1021/ja02242a004

Laysandra L, Ondang IJ, Ju Y-H, Ariandini BH, Mariska A, Soetaredjo FE, Putro JN, Santoso SP, Darsono FL, Ismadji S (2019) Highly adsorptive chitosan/saponin-bentonite composite film for removal of methyl orange and Cr(VI). Environ Sci Pollut Res 26:5020–5037. https://doi.org/10.1007/s11356-018-4035-2

Li N, Bai R (2005) Copper adsorption on chitosan-cellulose hydrogel beads: behaviors and mechanisms. Sep Purif Technol 42:237–247. https://doi.org/10.1016/j.seppur.2004.08.002

Liu M, Deng Y, Zhan H, Zhang X (2002) Adsorption and desorption of copper(II) from solutions on new spherical cellulose adsorbent. J Appl Polym Sci 84:478–485. https://doi.org/10.1002/app.10114

Lu F, Huang C, You L, Wang J, Zhang Q (2017) Magnetic hollow carbon microspheres as a reusable adsorbent for rhodamine B removal. RSC Adv 7:23255. https://doi.org/10.1039/c7ra03045b

Merrifield JD, Davids WG, MacRae JD, Amirbahman A (2004) Uptake of mercury by thiol-grafted chitosan gel beads. Water Res 38:3132–3138. https://doi.org/10.1016/j.watres.2004.04.008

Mohammadi T, Moheb A, Sadrzadeh M, Razmi A (2004) Separation of copper ions by electrodialysis using Taguchi experimental design. Desalination 169:21–31. https://doi.org/10.1016/j.desal.2004.08.004

Ngah WSW, Fatinathan S (2008) Adsorption of cu(II) ions in aqueous solution using chitosan beads, chitosan-GLA beads and chitosan-alginate beads. Chem Eng J 143:62–72. https://doi.org/10.1016/j.cej.2007.12.006

Nunthanid J, Puttipipatkhachorn S, Yamamoto K, Peck GE (2001) Physical properties and molecular behavior of chitosan films. Drug Dev Ind Pharm 27:143–157. https://doi.org/10.1081/DDC-100000481

Nyairo WN, Eker YR, Kowenje C, Akin I, Bingol H, Tor A, Ongeri DM (2018) Efficient adsorption of lead (II) and copper (II) from aqueous phase using oxidized multiwalled carbon nanotubes/polypyrrole composite. Sep Sci Technol 53:1498–1510. https://doi.org/10.1080/01496395.2018.1424203

Sankararamakrishnan N, Sanghi R (2006) Preparation and characterization of a novel xanthated chitosan. Carbohydr Polym 66:160–167. https://doi.org/10.1016/j.carbpol.2006.02.035

Santore RC, Di-Toro DM, Paquin PR, Allen HE, Meyer JS (2001) Biotic ligand model of the acute toxicity of metals. 2. Application to acute copper toxicity in freshwater fish and daphnia. Environ Toxicol Chem 20:2397–2402. https://doi.org/10.1016/S1462-9011(00)00047-2

Sotomayor FJ, cychosz KA, Thommes M (2018) Characterization of micro/mesoporous materials by Physisorption: concepts and case studies. Acc Mater Surf Res 3:34–50

Torres-Caban R, Vega-Olivencia CA, Alamo-Nole L, Morales-Irizarry D, Roman-Velazquez F, Mina-Camilde N (2019) Removal of copper fromWater by adsorption with calcium-alginate/spent-coffee-grounds composite beads. Materials 12:395. https://doi.org/10.3390/ma12030395

Turkington RW, Tracy FM (1958) Spectrophotometric determination of Ultramicro amounts of copper with 1,5-Diphenylcarbohydrazide. Anal Chem 30:1699–1701. https://doi.org/10.1021/ac60142a040

Yu J, Zheng J, Lu Q, Yang S, Wang X, Zhang X, Yang W (2016) Reusability and selective adsorption of Pb^{2+} on chitosan/P(2-acryl amido-2-methyl-1-propanesulfonic acid-*co*-acrylic acid) hydrogel. Iran Polym J 25:1009–1019. https://doi.org/10.1007/s13726-016-0487-8

Zhou L, Wang Y, Liu Z, Huang Q (2009) Characteristics of equilibrium, kinetics studies for adsorption of hg(II), cu(II), and Ni(II) ions by thiourea-modified magnetic chitosan microspheres. J Hazard Mater 161:995–1002. https://doi.org/10.1016/j.jhazmat.2008.04.078

Zhou L, Huang Y, Qiu W, Sun Z, Liu Z, Song Z (2017) Adsorption properties of Nano-MnO2–biochar composites for copper in aqueous solution. Molecules 22:173. https://doi.org/10.3390/molecules22010173